Oceanologia (2018) 60, 527—543

Available online at www.sciencedirect.com

ScienceDirect

journal homepage: www.journals.elsevier.com/oceanologia/

ORIGINAL RESEARCH ARTICLE

Narrowband shortwave minima of multispectral reflectance as indication of algal blooms associated with the mesoscale variability in the Brazil-Malvinas Confluence☆

Genrik S. Karabashev*, **Marina A. Evdoshenko**

Laboratory of Ocean Optics, Shirshov Institute of Oceanology RAS, Moscow, Russia

Received 5 February 2018; accepted 13 April 2018
Available online 30 April 2018

KEYWORDS
Algae;
Bloom;
Pigments;
Reflectance spectrum;
MODIS;
Brazil-Malvinas Confluence

Summary We examine the narrowband shortwave minima (NSM) of multispectral reflectance as indication of mesoscale algal blooms. They are frequent in the Brazil-Malvinas confluence zone (BMCZ) where our testing site (TS) belongs. Its MODIS A images of December 2008 and 2014 were the source of initial data. Classification of reflectance spectra in these images revealed that the TS look from space was determined by the most populated cluster of pixels having the only NSM at 443 nm. We divided this cluster into sub-clusters by maximum wavelengths λ_{max} from 412 to 555 nm and retrieved the estimates of λ_{max} (proxy for abundance of colored dissolved organic matter (CDOM)), chl_a (MODIS chlorophyll), R_{rs} (555) (turbidity proxy), and C_{ALH} (NSM-based chlorophyll) on a pixel-by-pixel basis. This allowed us to demonstrate: (1) the NSM magnitude at 443 nm peaked in mesoscale structures, (2) C_{ALH} was consistent with chlorophyll in the BMCZ waters samples, (3) positive linear correlation of R_{rs} (555) and C_{ALH} was characteristic of the TS waters at any λ_{max}, (4) the MODIS *chl_a* was overestimated when $\lambda_{max} > 488$ nm, (5) localization and outlines of mesoscale structures agreed well in the fields of pairs $R_{rs}(555) - C_{ALH}$ and $\lambda_{max} - chl\_a$, but not in the $C_{ALH} - chl\_a$ pair. The NSM-based chlorophyll C_{ALH} outperformed the

☆ Part of the paper was presented at the 9th International Conference "Current Problems in the Optics of Natural Waters", St. Petersburg, Russia, 20—22 September 2017.

* Corresponding author at: Laboratory of Ocean Optics, Shirshov Institute of Oceanology RAS, 36, Nahimovskiy prospekt, 117997 Moscow, Russia. Tel. +79672134331.
E-mail address: genkar@mail.ru (G.S. Karabashev).

Peer review under the responsibility of Institute of Oceanology of the Polish Academy of Sciences.

Production and hosting by Elsevier

https://doi.org/10.1016/j.oceano.2018.04.003

standard *chl_a* determinations in exactness because the C_{ALH} is insensitive to CDOM. This is advantageous when studying the Case 1 waters of intensive mesoscale variability where chlorophyll co-exists with the CDOM from eddy-induced blooms.

1. Introduction

In terms of semi-analytical approach (Morel et al., 2007), reflectance R_{rs} of a water body is a function of backscattering coefficient b_b and absorption coefficient a

$$R_{rs} = f[b_b/(a + b_b)]. \quad (1)$$

In Eq. (1), dimensionless factor f accounts for characteristics of incident radiance field and all members of Eq. (1) depend on wavelength λ. Every coefficient involves components that correspond to backscattering or absorption of solar radiation by different constituents of seawater. Therefore, we can write $b_b = b_{bp} + b_{bw}$ having in mind suspended particles of any origination (b_{bp}) and water proper (b_{bw}) as contributors into backscattering. Similarly, $a = a_{CDOM} + a_{ph} + a_m + a_w$ where a_{CDOM} is the absorption coefficients of CDOM (Colored Dissolved Organic Matter (Jerlov, 1976; Kalle, 1963)), a_{ph} represents the absorption of phytoplankton pigments in particles of biological origin, a_m characterizes absorption of mineralized particles of different nature, and a_w is the absorption coefficient of water proper. Hence, according to Eq. (1), the reflectance spectrum of water surface has to exhibit the maximums at wavelengths of maximal backscattering by particles and/or the minimums at wavelengths of maximal absorption by colored admixtures. In the context of remote sensing of water bodies, these relations are of interest exclusively in the visible because water severely attenuates UV and IR radiation.

Among the items of total absorption coefficient a, the pigment absorption a_{ph} is the only component whose wavelength dependence exhibits spectral bands much narrower than the visible range. High spectral selectivity of pigment absorption is advantageous in terms of analytical applications. This is the more so that the absorption of light by pigments directly depends on their content in water (Wozniak and Dera, 2007). Thus, it is reasonable to use a reflectance minimum at wavelength of maximal pigment absorption for retrieving the content of pigments from reflectance spectra of water surface.

Earlier studies (Jerlov, 1976) and current research (Stramski et al., 2004) provide no evidence that backscattering water constituents of any origination are able to mask the minimums of pigment absorption in seawater. The universal exponential growth of a_{CDOM} with diminishing wavelength of light (Jerlov, 1976; Nelson et al., 2010) does not preclude discrimination of a narrow-band reflectance pigment minimum. No fine structure of reflectance components due to mineral particles (a_{sm}) has been reported in Wozniak and Stramski (2004). Absorption spectrum of water proper is free of fine structure extremums too (Pope and Fry, 1997).

Based on the data of an airborne spectroradiometer, it has been found that the Sargasso Sea reflectance spectra are deprived of reflectance minima caused by pigment absorption (Clarke et al., 1970) which contradicts to what one might expect proceeding from the expression Eq. (1). The authors had noted that the shape of reflectance spectra was changing with the chlorophyll content and proposed to use this dependence for remote determination of chlorophyll.

The proposition was taken up and transformed into the concept of Case 1/Case 2 waters (Mobley et al., 2004; Morel, 1988, 2009). The latter implies that chlorophyll content in seawater is retrievable from the shape of reflectance spectra of water bodies whose optics depends exclusively on local phytoplankton abundance (Case 1 waters, mainly high seas) otherwise additional information is needed (Case 2 waters). This approach has been embodied in band-ratio algorithms. Since late 1970s to the present, this was the main avenue of remote sensing the chlorophyll in seas and oceans by means of multispectral ocean color scanners (Blondeau-Patissier et al., 2014; McClain, 2001).

The shipborne hyperspectral radiometers were widely used for groundtruthing the data of these instruments. Two outcomes of this activity are relevant to the present study. First, the content of chlorophyll in water retrieved with the help of band-ratio algorithms from multispectral reflectance tends to be over- or underestimated as compared to the ground truth data (Blondeau-Patissier et al., 2014; d'Ortenzio et al., 2002; Garcia et al., 2005). Second, the shortwave reflectance minima at wavelengths of maximal pigment absorption sometimes occurred in the open seawaters when measured with a hyperspectral shipborne radiometers (Kopelevich et al., 2005; Lubac and Loisel, 2007).

The first item is at least partially attributable to the fact that a band ratio algorithm is based on empirical dependence of ratio of reflectances loosely related to optical properties of chlorophyll. The second item hints to take advantage of absorption bands of chlorophyll and accessory pigments. According to expression Eq. (1), the presence of pigments in water manifests itself in minima of reflectance at wavelengths of absorption band maximums (reflectance deficit due to absorption). These bands peak mainly at $\lambda < 550$ nm (Wozniak and Dera, 2007). We named respective reflectance deficits as Narrowband Shortwave Minima (NSM) to highlight basic difference of our approach from band-ratio algorithms relying on reflectances of much wider spectral range.

Remote sensing at $\lambda < 550$ nm secures the deepest penetration of solar radiation in ocean water of high and moderate transparency (see Table XXVI in Jerlov, 1976). It is advantageous that the amplitude of the absorption bands of algal chlorophyll and respective NMS are directly proportional to the content of a pigment in algal cells in the absence of packaging and other secondary effects. These prospects are quite feasible in the case of an orbiting hyperspectral sensor. Yet, there are no indications that sensors of this kind are able

to become comparable to the multispectral ones in global coverage, revisit time, and availability of data collected.

When studying the cyanobacterial blooms in the Baltic Sea (Stal et al., 2003) from the data of multispectral sensor MODIS-Aqua, we have found numerous manifestations of NMS at 443 nm in the area of intensive blooming (Karabashev and Evdoshenko, 2015a). Based on the same approach, we observed similar NMS in transparent waters of the Southwest Tropical Pacific (Karabashev and Evdoshenko, 2015b) where cyanobacterial blooms were documented by conventional means (Dupouy et al., 2011). The same reflectance minima at different $\lambda < 550$ nm were observable in waters of the Patagonian shelf (Karabashev and Evdoshenko, 2016) noted for the diversity of algal species (Moreno et al., 2012), in the Caspian Sea (Karabashev and Evdoshenko, 2017a) and the Kerguelen Plateau in the Indian Ocean (Karabashev and Evdoshenko, 2017b) where water dynamics stimulates the protista bloom (Georges et al., 2014; Park et al., 2008).

The above blooms in the Baltic and Caspian Seas and at the Southwest Tropical Pacific Ocean were due to species of cyanobacteria. They are able to control their buoyancy and to accumulate near the air-water interface. The Kerguelen Plateau locates at latitude of the Circumpolar Current. It has been shown that internal tides promote here local vertical mixing and upward transfer of iron while general ocean circulation may foster the annual recurrence of blooms observed over the plateau (Park et al., 2008). Thus, different mechanisms support the surfacing of phytoplankton and make it visible as the NMS inherent to chlorophyll.

This inference prompted us to search for another mechanism of chlorophyll surfacing because none of the above ones is appropriate in the cases of reflectance deficit at 443 nm found in MODIS imagery east of the Patagonian shelf-break (Karabashev and Evdoshenko, 2016). This is the Brazil-Malvinas confluence zone (BMCZ) known for considerable variability of water surface reflectance (Acha et al., 2004; Garcia et al., 2008; Matano et al., 2010; Telesca et al., 2018) and characteristics of algal abundance and species diversity (d'Ovidio et al., 2010; Ferreira et al., 2013; Garcia et al., 2008). "The collision of the Brazil and Malvinas currents spawns one of the most spectacular eddy fields of the global ocean. The generation of warm- and cold-core eddies at either side of the front have led to mesoscale variability only matched by the offshore extensions of the Gulf Stream, the Kuroshio, and the Agulhas Current" (Piola and Matano, 2001).

The area of such oceanological intricacy is the most appropriate place for attaining our aim: to reveal the potential of narrowband shortwave minima (NSM) of multispectral satellite reflectance as indication of chlorophyll abundance related to the mesoscale variability in Case 1 waters.

2. Background, methods, and materials

2.1. Testing site

Fig. 1 gives an idea of basic features of the BMCZ and positioning of the testing site (TS) relative expectable sources of mesoscale variability.

(a) Potential temperature θ of the Malvinas Current grows from 4°C at ~56°S to 16°C at ~40°S (Fig. 1) where it turns back under the action of warmer Brazil Current ($\theta > 20$°C) according to Piola and Matano (2001). This promises intensive mesoscale between-currents water exchange observable in remotely sensed fields of optical characteristics and SST.

(b) Interaction of the Malvinas Current and continental slope is hypothetically one of potential triggers of mesoscale variability of water properties along the route of the Malvinas Current.

(c) The Malvinas Current flows around the Malvinas Archipelago, which may trigger the mesoscale island wakes to the north of the latter. The island-generated eddies are characteristic of deep ocean islands in the paths of currents (Barton, 2001).

(d) A shelfbreak upwelling is a permanent feature of the study area (Matano and Palma, 2008). The upwelling is visible in satellite distributions of SST and reflectance as a narrow stripe where isobaths 150–1000 m in Fig. 1 come closer together. To all appearance, the upwelling and northbound general transport of shelf waters prevents intrusion of the latter to the east of the shelfbreak.

To summarize, the testing site area to the east of the shelfbreak (Fig. 1) is a natural model of Case 1 water

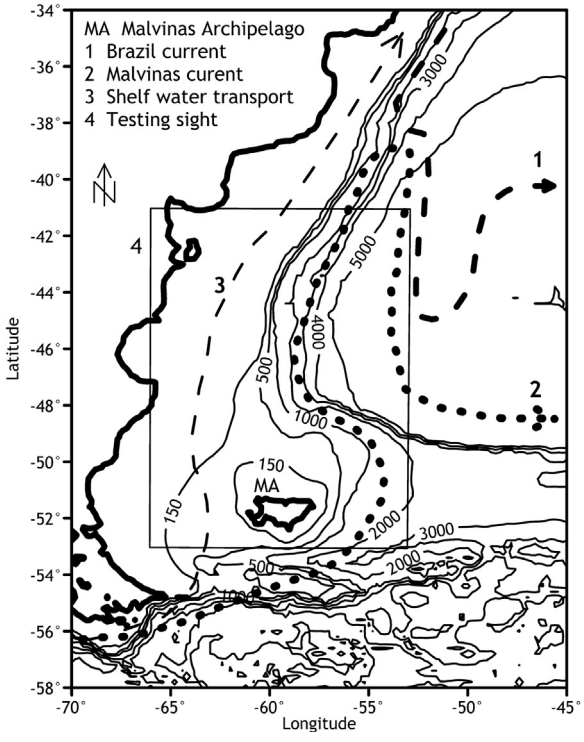

Figure 1 Study area, its bottom relief, and quasi-permanent water flows 1–3 in the BMCZ reproduced from patterns in (d'Ovidio et al., 2010; Loder et al., 1998; Matano et al., 2010; Piola and Matano, 2001). The bold lines indicate the land-water interface. Testing site 4 designates the limits of satellite images used as a source of initial data on reflectance and SST. Here and in the following figures, the isobaths are plotted from the bathymetry gridded with the help of GEBCO Grid Demonstrator (https://www.bodc.ac.uk/).

body were intensive mesoscale variability is a common phenomenon.

2.2. Approach

2.2.1. Sensor

The mesoscale inhomogeneities, being anything from 10^1 to 10^2 km in size and from a few days to a few weeks in time, are considered as fluid dynamical niches of phytoplankton types in the ocean (d'Ovidio et al., 2010). These scales and periods match the specifications of any multispectral orbiting sensor. However, the Moderate Resolution Imaging Spectroradiometer (MODIS) is the most advantageous one for our goals.

MODIS is the only sensor whose set of spectral channels at λ = 412, 443, 469, 488, 531, 547, 555, 645, 667, and 678 nm permits, to an extent, to discriminate reflectance deficit due to shortwave absorption bands of chlorophyll and accessory pigments in phytoplankton cells. The 443 nm channel is tuned to the absorption peak of chlorophyll *a* (Soret band). Hence, reflectance minimum at 443 points to chlorophyll in water regardless of spectrum shape. Reflectance minimum at 488 nm is attributable to the same band of other chlorophylls and/or accessory pigments of phytoplankton (Wozniak and Dera, 2007), while broader reflectance minimum from 412 to 555 nm is probable when diversity of pigments in local phytoplankton is at its maximum. The study area is known as a region of widely varying species composition of phytoplankton population (d'Ovidio et al., 2010; Garcia et al., 2008). It is advantageous that the archive of MODIS global imagery covers the period from 2002 to the present and MODIS images provide global coverage at GSD = 1 km.

2.2.2. Absorption line of chlorophyll as an indication of its content in water

Index D1 = $R_{rs}(412) - R_{rs}(443)$ has been proposed as a simplest quantitative measure of chlorophyll content in water based on reflectances deficit at 443 nm (Karabashev and Evdoshenko, 2015b). In inland seas, reflectance spectra peak at $\lambda_{max} > 469$ nm and D1 < 0. Linear dependence of D1 upon chlorophyll content has been established from the Caspian Sea data (Karabashev and Evdoshenko, 2016). However, the index D1 becomes positive in transparent ocean waters where λ_{max} = 412 nm. Now we eliminate this inconvenience and propose a new universal chlorophyll index. It is designated the Absorption Line Height of chlorophyll (ALH) by analogy with the Fluorescence Line Height (FLH) of the same pigment (Letelier and Abbott, 1996). We calculate ALH pixel-by-pixel through the linear interpolation

$$\mathrm{ALH} = R_{rs}(412) + 0.54 \times [R_{rs}(469 - R_{rs}(412)] - R_{rs}(443). \quad (2)$$

Additional goal of the present study is to examine the diagnostic potential of the ALH index.

2.3. Optical characteristics of phytoplankton blooming

In the context of ALH examination, characteristic no. 1 should be the satellite concentration of chlorophyll *chl_a*. It is retrieved with the help of the OCI algorithm for Case 1 waters (Hu et al., 2012) and available as a level L2 standard product of MODIS sensors along with the estimates of chlorophyll *chl_ocx* based on the OCX algorithm. According to Hu et al. (2012), *chl_ocx* is inferior to *chl_a* in accuracy of retrieval of chlorophyll concentration in ocean waters.

Proportionality of absorption of chlorophyll to its content in water justifies the use of a simple formula for converting ALH into chlorophyll concentration C_{ALH} as a trial solution:

$$C_{ALH} = 12 \times \mathrm{ALH} + 0.106. \quad (3)$$

Expression (3) is based on the data of MODIS-A image of anticyclonic eddy at the Southern Caspian Sea (September 1, 2005). The regional algorithm (Kopelevich et al., 2013) for chlorophyll retrieving and expression (2) for ALH determination were used to obtain regression (3) at R^2 = 0.92.

Having regard to the fact that reflectance $R_{rs}(555)$ belongs to the spectral range of minimal absorption of light by CDOM and water proper (Jerlov, 1976), we use $R_{rs}(555)$ as an index of relative abundance of suspended light-scattering particles in a layer of origination of water-leaving radiance. The scattering coefficient b_b is more appropriate here, but it is hardly possible to calculate it from reflectance at satisfactory accuracy in waters widely varying in size, density, composition, and vertical distribution of suspended particles.

The MODIS spectral channels allow one to discriminate the ocean waters in relative abundance of CDOM: the higher is CDOM content in water, the closer is λ_{max} to 555 nm because of expression (1) and exponential growth of a_{CDOM} with diminishing λ (Jerlov, 1976). This dependence is helpful for typifying the ocean waters from λ_{max}. The latter is higher in areas where CDOM attenuates the shortwave reflectance stronger than it is contributed by backscattering of suspended matter. The advantage of λ_{max} is in the fact, that it is defined by MODIS design without relying on questionable assumptions and is universally applicable in ocean waters of low and moderate biological productivity.

2.4. Initial data

The season of maximum insolation of ocean surface and lowest losses of data due to cloudiness, Sun glint, and other inferences — these were the main criteria for selecting the images of the testing site. These conditions turned out to be too severe to compose series of images of the testing site for assessing seasonal changes in distributions of characteristics involved. However, tolerance to data gaps hampers identification of mesoscale events in individual images of the testing site. This is of primary importance for the present work.

Use has been made of the browser at http://oceancolor.gsfc.nasa.gov/ (NASA) to select and download the data of level L2 of MODIS Aqua in more than 20 images of the testing site obtained in December–January from 2004 to 2016. Final selection of images was performed with the help of SMCS browser (Sheberstov, 2015). The latter supports batch processing and visualization of data of many orbital sensors, allows to eliminate pixels corrupted by cloudiness, Sun glint, and other inferences and to export the pre-processed data for further treatment. In the present study, we exported reflectance R_{rs} at 412, 443, 469, 488, 531, 547, 555, 620, 645 and 678 nm and estimates of chlorophyll concentration *chl_a*, found with the

standard MODIS algorithm OCI (Hu et al., 2012). Error-free distributions of SST, obtained by MODIS sensor concurrently with optical information, were also exported from the SMCS browser. Finally, we restricted our choice to scenes A2014336182000.L2_LAC_OC.nc, A2014336182000.L2_LAC_SST.nc, A2008341184000.L2_LAC_OC.nc, A2008341184000.L2_LAC_SST.nc, A2008345181500.L2_LAC_OC.nc, and A2008345181500.L2_LAC_SST.nc. They were downloaded on July 5, 2017, from the US NASA OBPG (http://oceancolor.gsfc.nasa.gov/) using reprocessing R2014.0, at GSD = 1 km.

2.5. Data processing

According to earlier experience (Karabashev and Evdoshenko, 2016), reflectance spectra of pixels in images of testing site widely vary in shape over the BMCZ. Therefore, we restricted our consideration to the specific type of reflectance spectrum having the only chlorophyll-inherent minimum at 443 nm. More complicated spectral shapes at $\lambda < 550$ nm should be attributed to co-occurrence of different pigments in water but scarcity of relevant information gives no way of identifying their nature at present.

The MATLAB scripts were the main tool for data treatment. It started from eliminating the pixels corrupted by cloudiness, Sun glint, outliers, and the like from files of every scene. Next was the stage of pixels classification by shape of reflectance spectrum. The logical sums of inequalities of adjacent R_{rs}, describing the shape of pixel's spectrum at $\lambda \leq 555$ nm, were applied to discriminate four clusters of pixels' spectra. For example, the sum $[(R_{rs}(412) > R_{rs}(443)) + (R_{rs}(469) > R_{rs}(443)) = 2]$ identified the pixels whose reflectance spectra exhibited the sole minimum at 443 nm.

The sum tuned to distinguish spectra of broad minimum at 469 nm from 412 to 531 nm identified the pixels of cluster no. 1. They were removed from the set of remaining pixels. Cluster no. 2 was recognized based on the sum tuned to spectral minima at 488 nm (obligatory) and 443 nm (optionally) and removed from the rest of pixels. The pixels of cluster no. 3 were identified using the sum tuned to the only minimum at 443 nm inherent to the chlorophyll. Cluster no. 4 involves remaining unidentified pixels. This operating sequence secures the absence of "foreign" pixels in spectra of cluster no. 3 and the absence of any shortwave minima in spectra of cluster no. 4. Now we subdivide the pixels of clusters no. 3 and no. 4 into respective sub-clusters by maximal wavelength of pixels' spectra at 412, 443, 469, 488, 531, 547, 555 nm. Finally, the attributes of every pixel in cluster no. 3 were added with the estimates of λ_{max}, ALH, and C_{ALH}, calculated from pixel's reflectances according to above considerations and expressions. In this way, we have

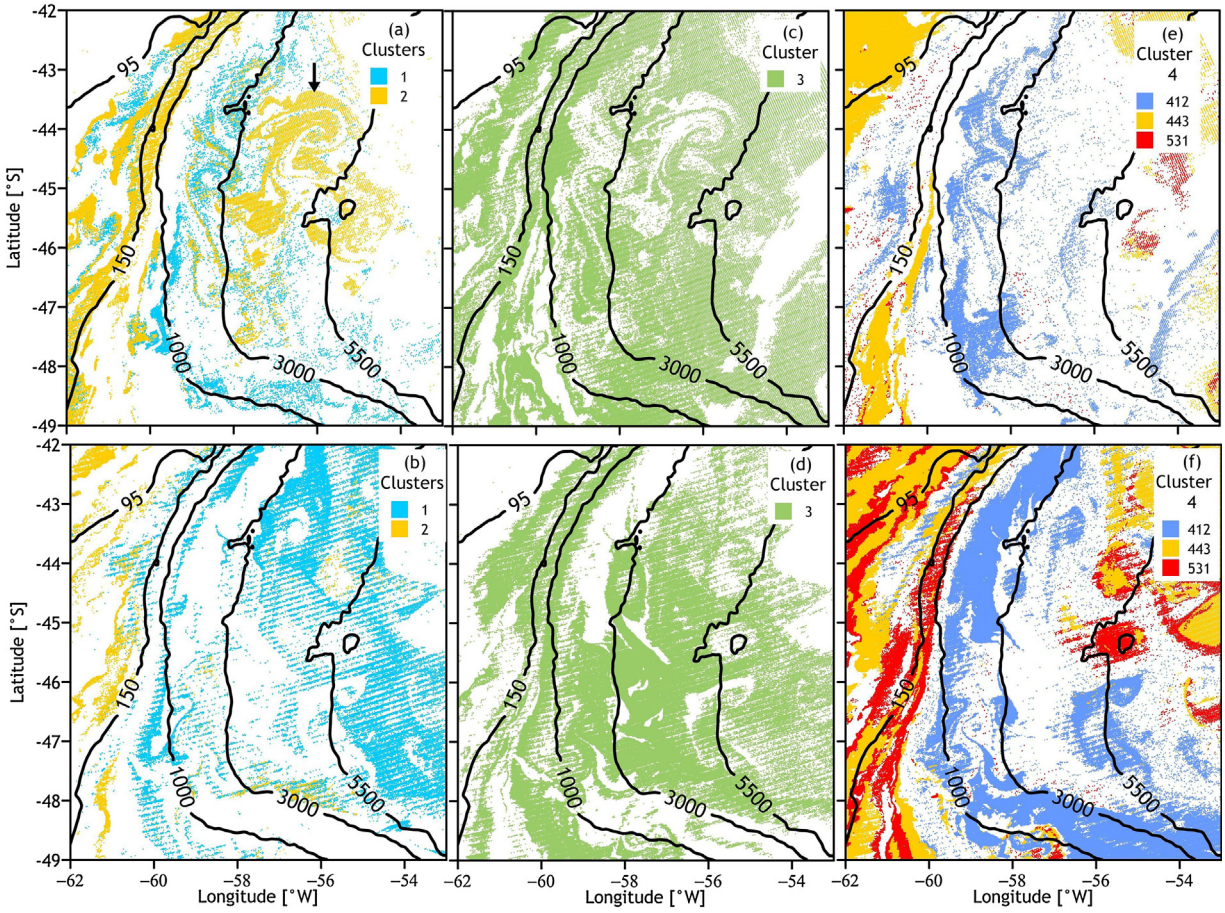

Figure 2 Distributions of pixels' clusters in testing sight images taken with the MODIS Aqua sensor on 2008-12-06 (panels (a), (c), (e)) and 2014-12-02 (panels (b), (d), (f)). Cluster 4 is divided into three sub-clusters by λ_{max} from 412 to 547 nm. For details see text.

prepared tables of reflectance data and derived quantities for dates 2008-12-06, 2008-12-10, and 2014-12-02 along with the SST tables for the same dates.

These tables were used for visualizing the distributions of quantities in question and for estimating their statistical characteristics. The visual perception of spatial patterns was particularly important because extensions of testing site allow us to observe the co-occurrence of different mesoscale events and their relation to the satellite SST distribution and the TS bottom relief.

3. Results

3.1. Distribution of spectral clusters

Fig. 2 shows the distributions of members of above spectral clusters over the TS fragment mapped from MODIS images of 2008-12-06 and 2014-12-02. The maps in Fig. 2 demonstrate spatial intermittency of spectrally different pixels at scales close to MODIS GSD = 1 km (submesoscale range). Nevertheless, there were spectrally uniform mesoscale structures. They are (i) the shelf to the west of 95 m isobath, where pixels of cluster no. 4 outnumber the spectra of other clusters, (ii) spaces between the 1000 and 3000 m isobaths, that are empty in maps (b) and (d) but filled with pixels of sub-cluster 412 of cluster no. 4 in map (f), (iii) in map (a) (arrow), the pixels of cluster no. 2 fill the empty places in outlines of an eddy dipole visible in map (c) between the 3000 m and 5000 m isobaths from 46.0°S to 43.5°S.

The population of cluster no. 3 is comparable to the total population of other clusters (Fig. 2). We focused on analyzing the data of cluster no. 3 for two reasons. First, being the most populated, it plays a leading role in shaping the patterns observable from space in testing site images. Second, it is a good probability that the NSMs in spectra of this cluster are uniquely determined by chlorophyll in water whereas the broad or multiple NSMs are due to pigments whose composition is difficult to establish without ground truthing information.

We divided the spectra of the cluster no. 3 into sub-clusters by λ_{max} (sc412, sc469, sc488, sc531, sc547, and sc555). Fig. 3 displays the average spectra of these sub-clusters calculated from the data that underlie the respective distributions of 2008-12-06 and 2014-12-02 in Fig. 2. In both cases, sub-cluster sc412 significantly surpassed the rest of sub-clusters in population, and sc531 was the second largest sub-cluster. Fig. 3 gives the idea of the NSM shape and shows significant inter-annual changes of spectral shapes in sub-clusters at the same λ_{max} and season.

3.2. Distributions of optical characteristics

The maps (a) and (b) in Fig. 4 demonstrate coincidence of localization and outlines of patches of higher λ_{max} and larger *chl_a* north of the Malvinas Archipelago and the X-shaped structure occurrence at 47°S east of the 4000 m isobath. These patchy structures are absent in maps (c) and (d). Here the areas of maximum estimates of $R_{rs}(555)$ and C_{ALH} coincide in part. The similarity of distributions in pairs λ_{max} — *chl_a* and $R_{rs}(555)$ — C_{ALH} survived in images of the same water area recorded a few days later (Fig. 5, panels (a),(b) and (c),(d)).

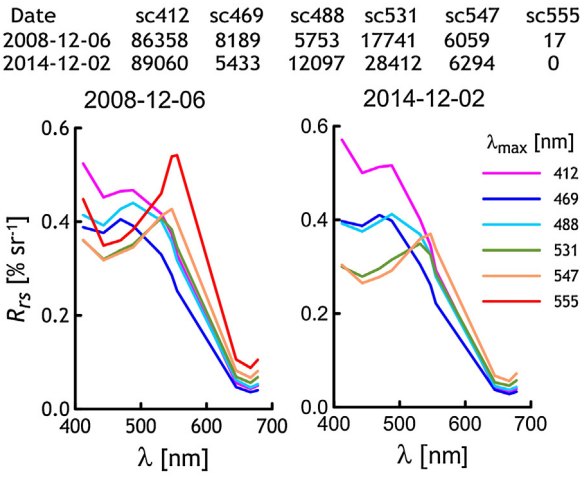

Figure 3 Population of sub-clusters sc412-sc555 of cluster no. 3 distinguished by wavelength λ_{max} from 412 to 555 nm (top) and average spectra of these sub-clusters (bottom) calculated from data underlying the maps of 2008-12-06 and 2014-12-02 in Fig. 2.

Figs. 6 and 7 show more radical interannual changes in the distributions of λ_{max}, *chl_a*, R_{rs} (555), and C_{ALH}. However, the similarity in paired distributions of λ_{max} — *chl_a* and R_{rs} (555) — C_{ALH} as well as the differences between the pairs took place too. The following facts came to our attention.

1. The highest levels of $R_{rs}(555)$ and C_{ALH} visualize compact eddy-like structures 1—3 in maps (c) and (d) of Fig. 6, but they are difficult to distinguish in panels (a) (λ_{max}) and (b) (*chl_a*) in the same maps.
2. In Fig. 6, the stripes of $\lambda_{max} \geq 531$ nm and moderate *chl_a* occur between the isobaths 500 and 1000 m (maps (a) and (b)) while elevated $R_{rs}(555)$ (c) and C_{ALH} (d) located between the 1000 and 2000 m isobaths.
3. In maps (a) and (b), Fig. 7, a distinctive structure *1* of intricate shape stands out against a background of 2000 m isobath between 47°S and 45°S. This structure is difficult to distinguish in maps (c) and (d).
4. A mesoscale circular structure *2* in maps (c) and (d) in Fig. 7 is easy to recognize thanks to maximal $R_{rs}(555)$ and NSM-chlorophyll, but the same places in maps (a) and (b) are occupied by the lowest estimates of λ_{max} and *chl_a*.

In order to clarify this facts, we have turned to MODIS-determinations of the SST in the testing site for the same date and time (scene A2014336182000.L2_LAC_SST.nc), and compared the outlines of inhomogeneities of SST and optical characteristics (Fig. 8). Here the pathway of the Malvinas Current is traced by the lowest SST. A loop-like structure L is a distinctive feature of distributions of SST (a), λ_{max} (b), and *chl_a* (c) to the south of 46°S. This structure is visualized by SST > 9.4°C and higher λ_{max} and *chl_a* (same maps). The highest contrast exhibits the distribution of λ_{max} where λ_{max} = 547 nm traces the loop itself against a background of pixels whose λ_{max} = 412 nm. This loop is traceable in the field of $R_{rs}(555)$ (e) and almost disappears in C_{ALH} distribution (f). The maps (d)—(f) demonstrate an eddy-like structure E marked by the highest $R_{rs}(555)$ and C_{ALH} and medium level SST.

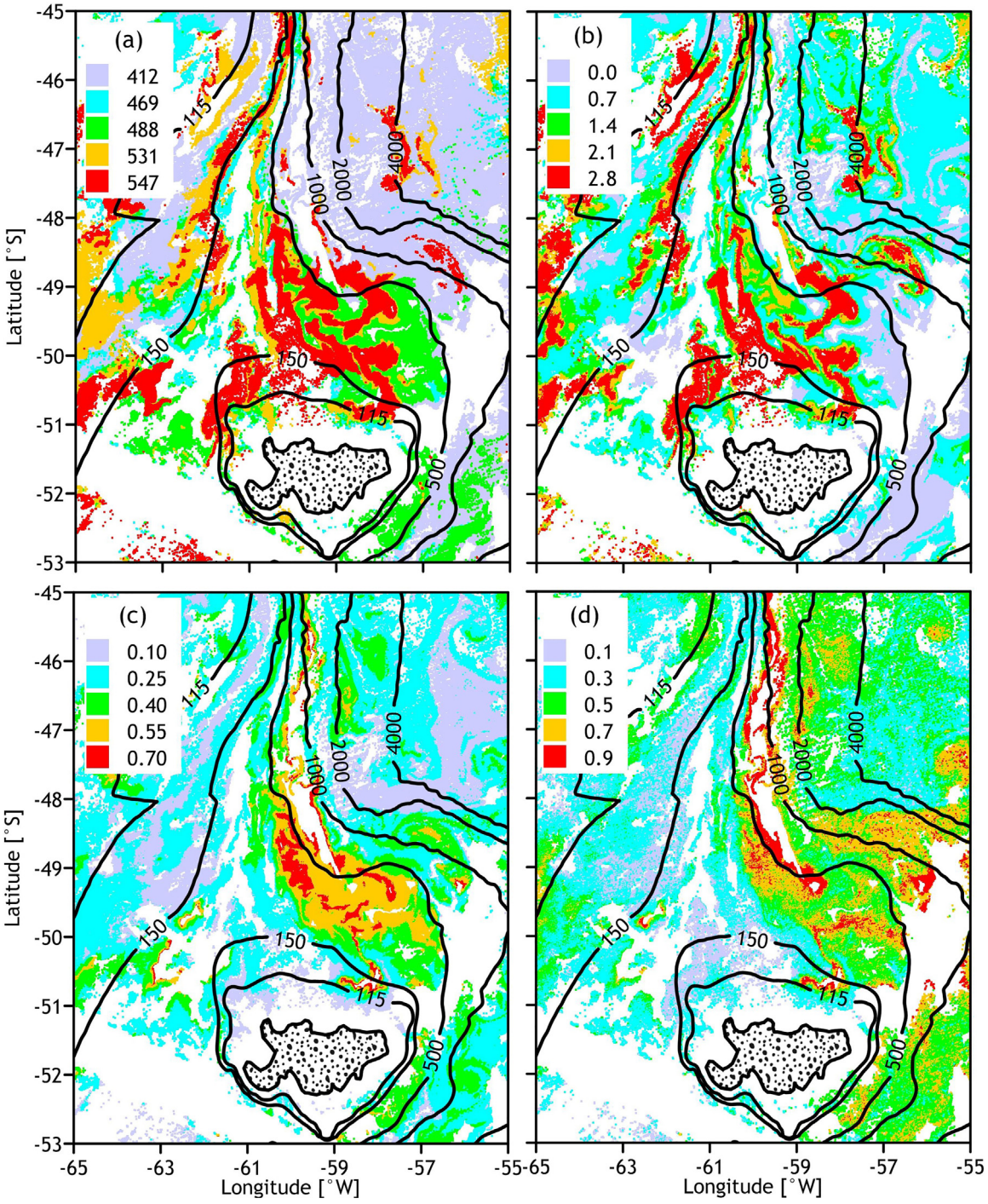

Figure 4 Pixel-by-pixel distributions of (a) wavelength of reflectance spectral maximum λ_{max} [nm], (b) MODIS chlorophyll *chl-a* [mg m^{-3}], (c) reflectance $R_{rs}(555)$ [% sr^{-1}], and (d) NSM-based chlorophyll C_{ALH} [mg m^{-3}]. They were plotted from pixels' attributes of the TS image of 2008-12-06.

3.3. Relationships of characteristics associated with suspended matter

The scatter of *chl_a* and C_{ALH} relative to the $R_{rs}(555)$ determinations (Fig. 9) provides impartial idea of inconsistency of chlorophyll concentrations retrieved from reflectance spectra of individual pixels' by means of MODIS algorithm or based on determinations of C_{ALH}. The graphs in Fig. 9 were plotted from the data of 2008-12-06 and 2014-12-02 and show that the changes in C_{ALH} and $R_{rs}(555)$ positively co-varied in both cases. Except for the subsample at λ_{max} = 469 nm, the estimates of *chl_a* changed chaotically relative to variations in $R_{rs}(555)$ under the same conditions.

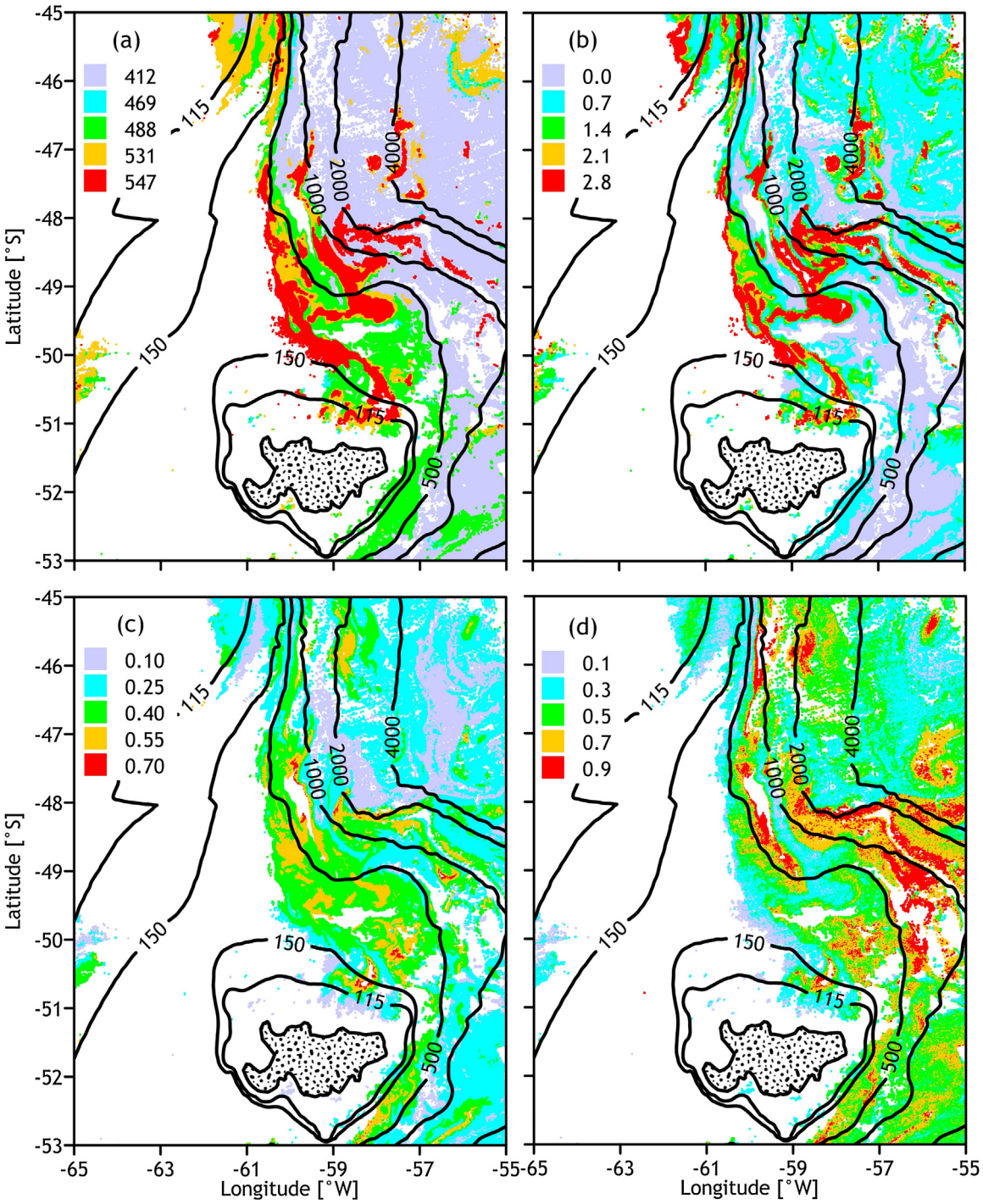

Figure 5 The same as in Fig. 4 but from the TS image of 2008-12-10. White spaces represent areas of missing data.

The histograms in Fig. 10 demonstrate the distributions of C_{ALH}, $R_{rs}(555)$, and *chl_a* in the sub-clusters of cluster no. 3 classed by λ_{max} and calculated from data of 2008-12-06 and 2014-12. The distributions of C_{ALH} belong to the common range of C_{ALH} estimates regardless of λ_{max}. The same behavior is evident in distributions of $R_{rs}(555)$. On the contrary, the histograms of *chl-a* tend to displace to higher *chl_a* subsequent to λ_{max} of pixel's spectrum.

4. Discussion

4.1. Surprising results in distribution and shape of reflectance spectra

The outcomes of clustering procedure seem acceptable with the exception of two results: spatial intermittency of spec-

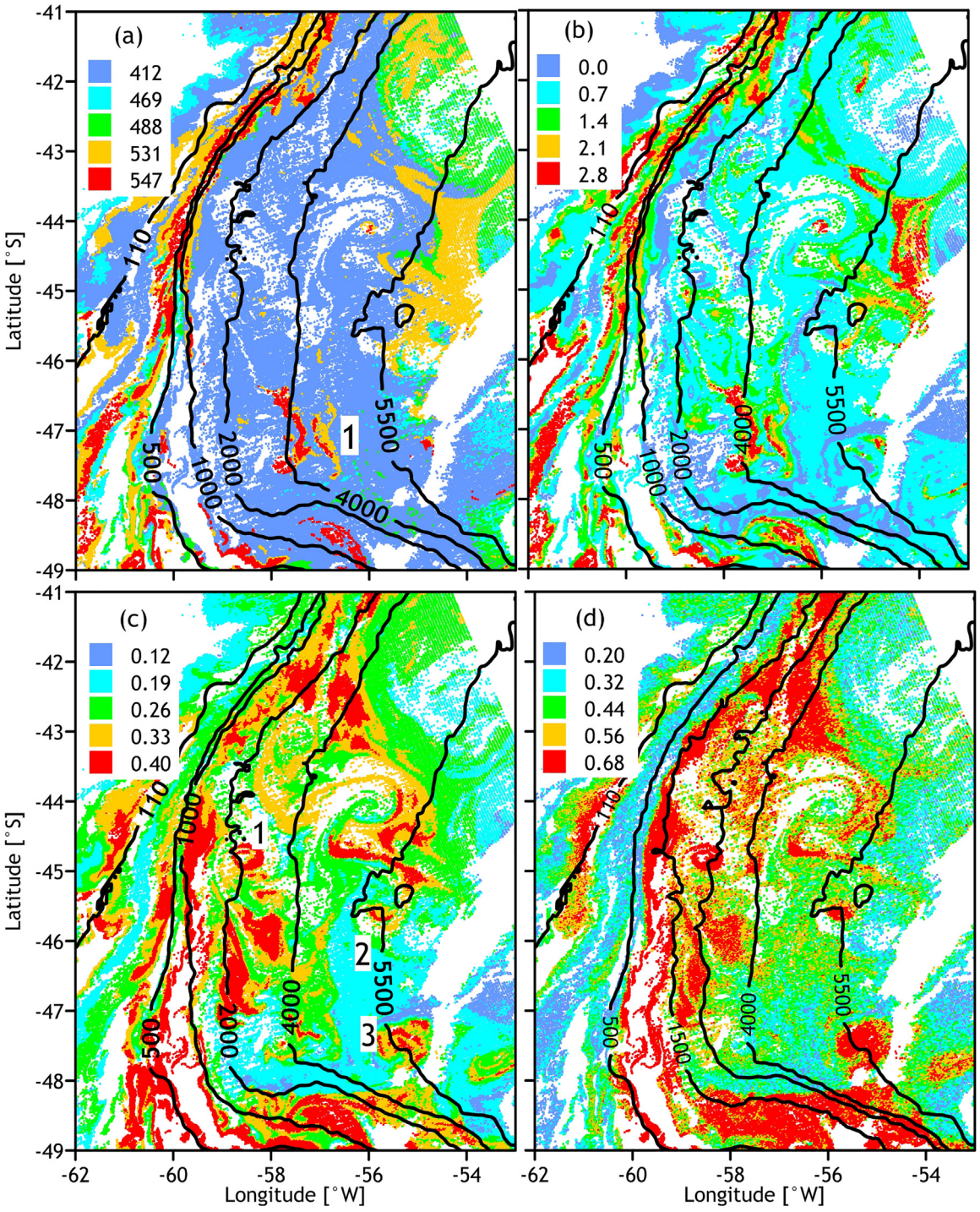

Figure 6 Pixel-by-pixel distributions of (a) wavelength of reflectance spectral maximum λ_{max} [nm], (b) MODIS chlorophyll *chl-a* [mg m^{-3}], (c) reflectance $R_{rs}(555)$ [% sr^{-1}], and (d) NSM-based chlorophyll C_{ALH} [mg m^{-3}] plotted from TS image of 2008-12-06. The distributions characterize the TS fragment shifted 4° to the north relative the TS fragment in Fig. 4. Figure-of-one in panel (a) indicates the X-like structure in panels (a) and (b). Figs. 1–3 in panel (c) mark circular structures similarly located in panels (c) and (d).

trally different pixels (Fig. 2) and widening of the shortwave minimum in spectra of sub-clusters of cluster no. 3 at $\lambda_{max} > 488$ nm (Fig. 3).

The intermittency of members of different spectral clusters is not a universal feature of the study area because large mesoscale structures comprise the pixels of the same spectral type (see Section 3.1). Supposedly, an illusory intermittency arises at places where NSM amplitude of pixels is close to zero. However, intermittency of reflectance spectra at scales below 10 km may be due to submesoscale forcings: "Submesoscale dynamics contribute to phytoplankton production by enhancing the supply of nutrients in regions that are nutrient limited and by generating density stratification in the surface layer to increase light exposure

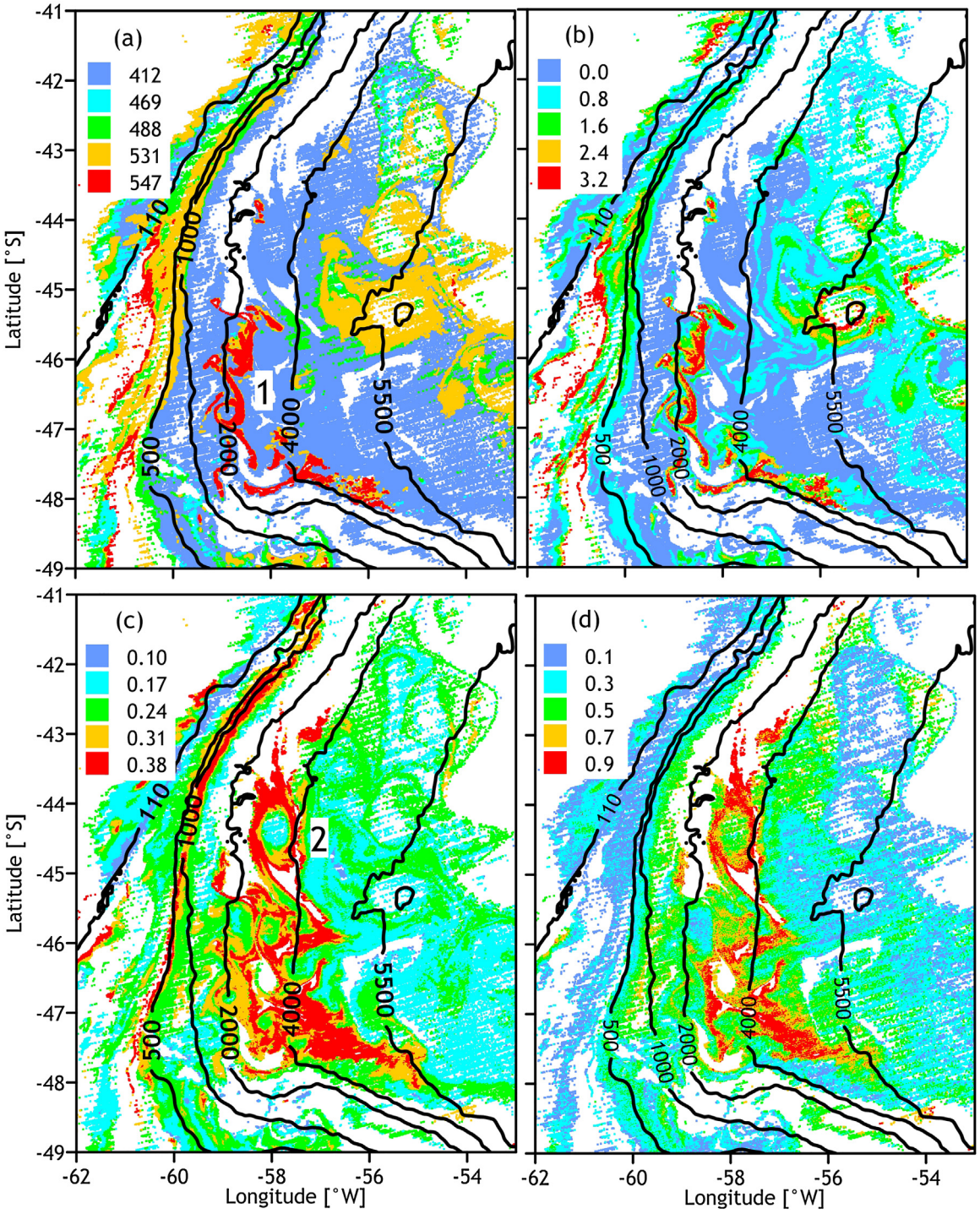

Figure 7 The same as in Fig. 6 but the maps were plotted from the TS image of 2014-12-02. The figure-of-one points to the similar mesoscale structures in panels (a) and (b) and figure-of-two indicates the eddy-like structure in panels (c) and (d).

for phytoplankton that are light limited. These effects occur locally at scales of 0.1–10 km and over a few days and result in the heterogeneous supply and distribution of nutrients, stratification, and mixed-layer depth, which generate patches of high productivity that are thought to contribute substantially to oceanic ecosystems, their structure and phenology, and the ensuing trophic cascades." (Mahadevan, 2016). The issue of spectral intermittency deserves a targeted study before it may be write off for experimental errors.

As for the widening of the NSM, it is evidently due to algal cells containing large quantities of accessory pigments along

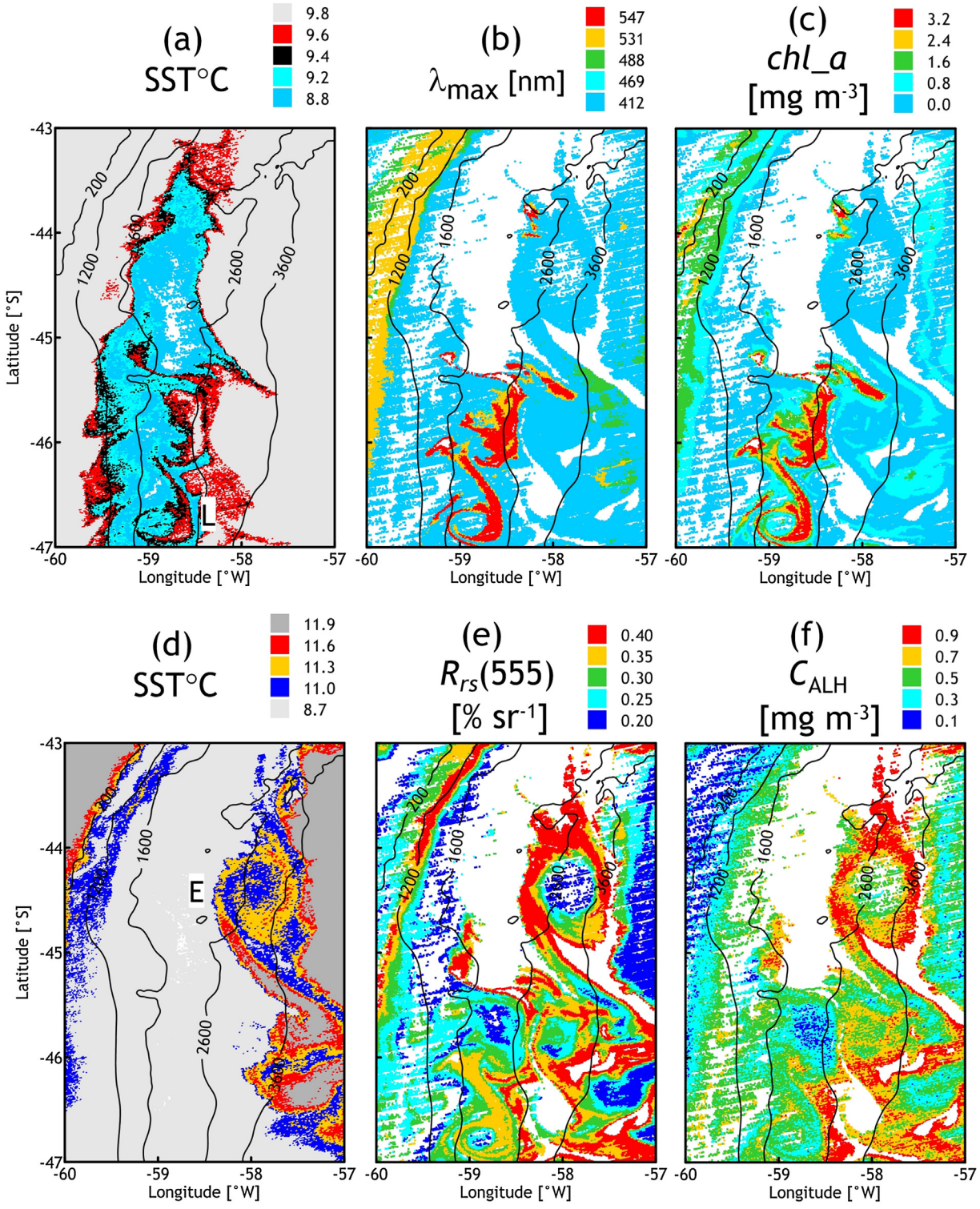

Figure 8 Distribution of SST ((a) and (d)) and bio-optical characteristics λ_{max} (b), *chl_a* (c), $R_{rs}(555)$ (e), and C_{ALH} (f) retrieved from attributes of pixels of cluster no. 3 in a fragment of testing site image of 2014-12-02. White spaces in maps (b), (c), (e), and (d) indicate missing data or pixels of clusters other than cluster no. 3.

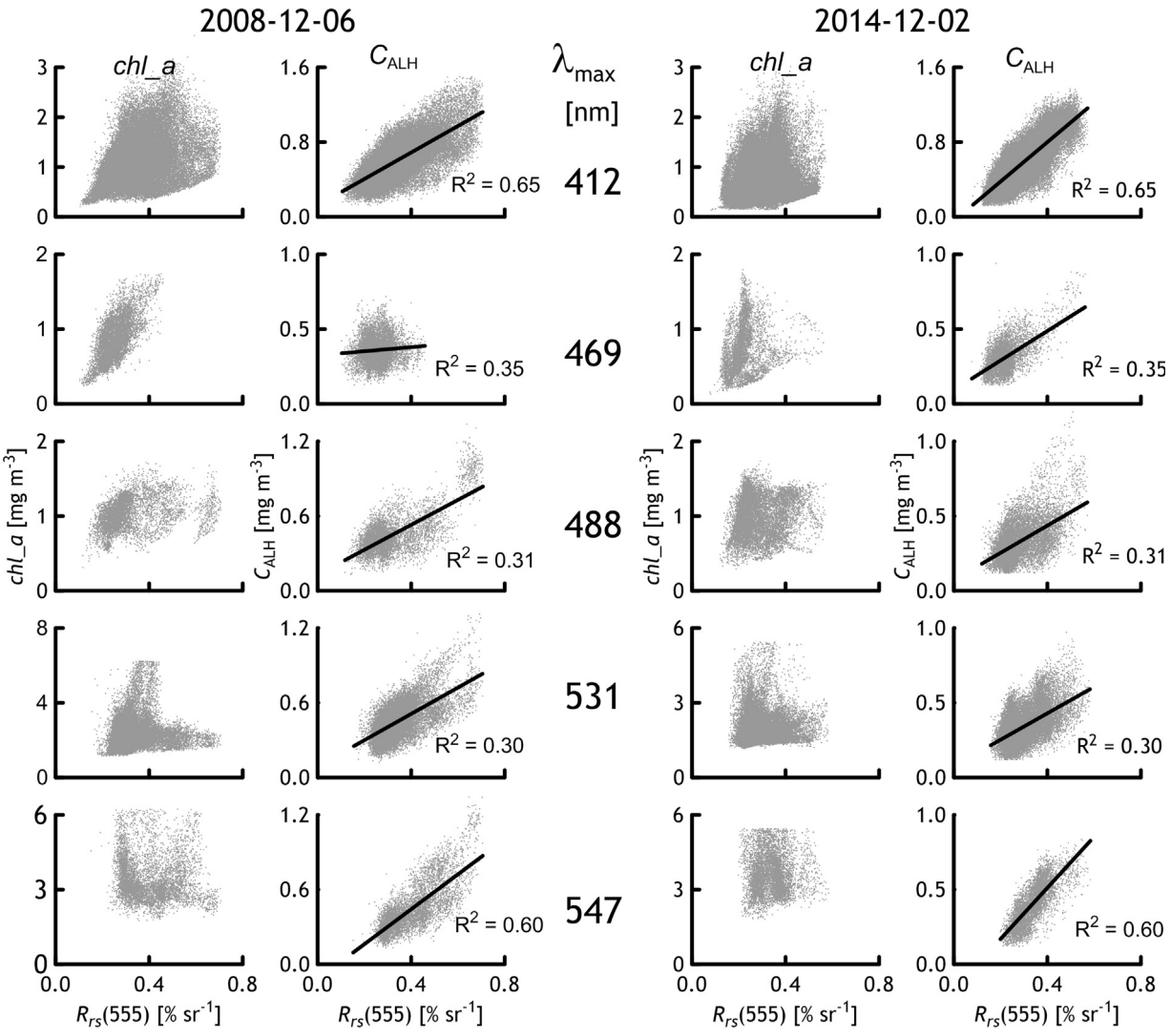

Figure 9 Plots of *chl_a* and C_{ALH} scatter relative to $R_{rs}(555)$. They are based on cluster no. 3 data divided into sub-clusters by wavelength of spectral maximums λ_{max} of pixels in images of 2008-12-06 (Fig. 6) and 2014-12-02 (Fig. 7). R^2 is the coefficient of determination.

with the chlorophyll *a*. Inability to resolve the combined reflectance spectrum of pigment mixture is a limitation inherent to the multispectral sensors.

4.2. Relation of C_{ALH} to bio-optical characteristics derivable from spectral reflectance

In a large natural water basin, unpredictable occurrence and relatively short residence time of mesoscale structures hamper the analysis of satellite data obtainable concurrently with a ship-borne and orbiting instruments. This sends us to a comparative qualitative analysis of C_{ALH} and well-understood quantities. To a first approximation, reflectance $R_{rs}(555)$ is a quantity determined by content of particles in water and independent of CDOM and phytoplankton pigments (Jerlov, 1976; Stramski et al., 2004). Therefore, $R_{rs}(555)$ may be regarded as an index of the water turbidity caused by suspended matter while C_{ALH} indicates the living particles. They are the main source of suspended matter of local origin in the shelf-break and adjacent waters and qualified as nanoplankton (Ferreira et al., 2013). Being larger than the wavelength of light (2 μm and more against $\lambda < 0.7$ μm), they non-selectively backscatter the solar radiation (Jerlov, 1976). Consequently, the CDOM and phytoplankton pigments are the main agents that dictate the shape of reflectance spectrum in the TS.

The linear relationship of C_{ALH} and $R_{rs}(555)$ in Fig. 9 agrees well with these considerations and the idea of ALH as a remote index of chlorophyll content in water. The coefficient of determination ranges from 0.30 to 0.65, points to moderately strong linear correlation of C_{ALH} with $R_{rs}(555)$, and appears quite expectable for genetically related but physically different substances. The graphs in Fig. 9 show that MODIS chlorophyll *chl_a* is unrelated to $R_{rs}(555)$ and to C_{ALH}. Chaotic scatter of *chl_a* relative to $R_{rs}(555)$ estimates is incompatible with the Case 1 water concept. The latter regards the algal mass as a sole source of suspended matter in water bodies free of sources of allochthonous optically

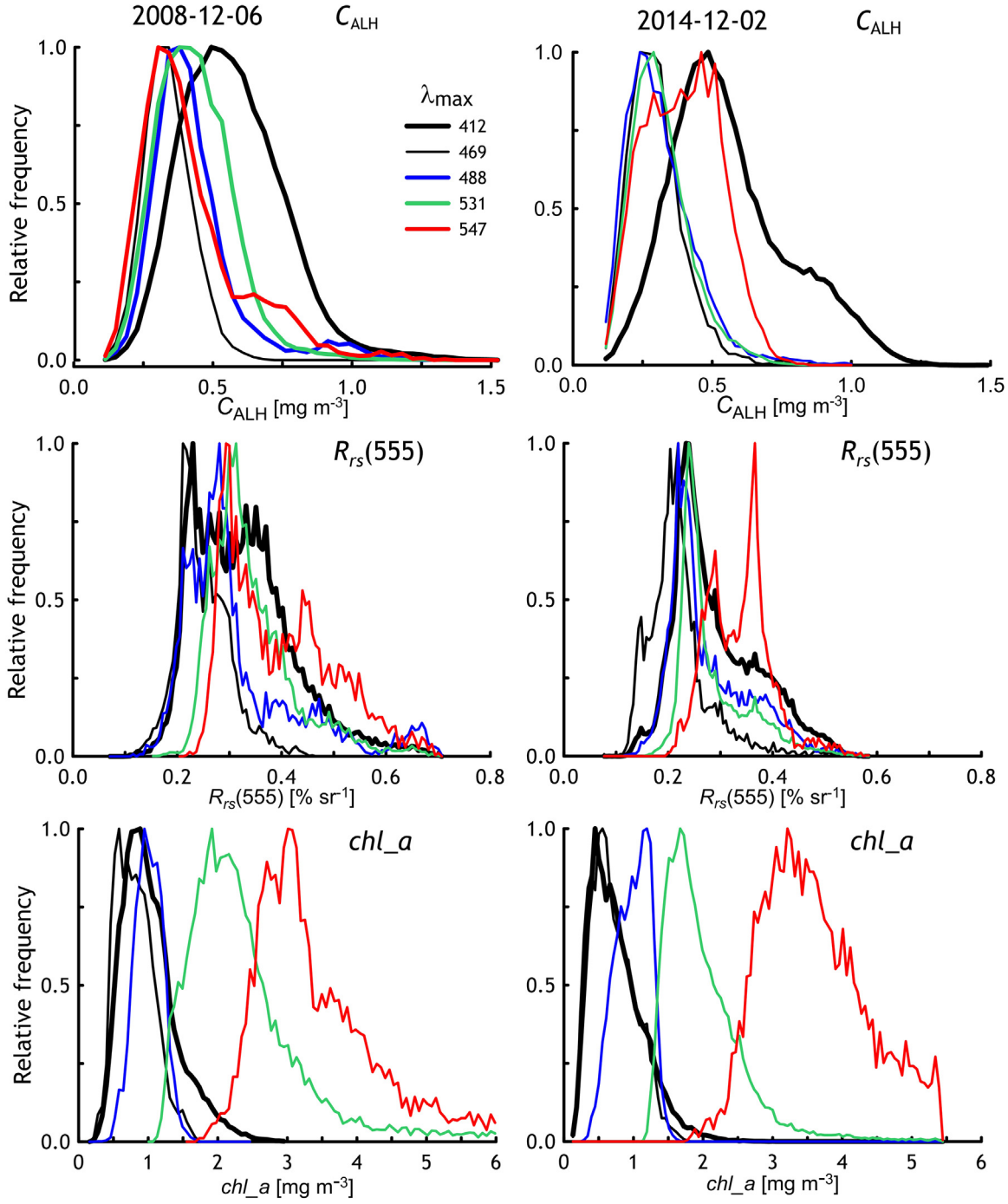

Figure 10 Relative frequencies of the estimates of NSM-chlorophyll C_{ALH}, reflectance R_{rs} (555), and MODIS chlorophyll *chl_a*. They rely on data of TS images taken by MODIS sensor for dates 2008-12-06 (Fig. 6) and 2014-12-02 (Fig. 7) and pertain to cluster no. 3 divided into sub-clusters by λ_{max} of reflectance spectra of individual pixels.

significant admixtures and is perfectly applicable to the BMCZ waters.

4.3. λ_{max} as an index of local relative abundance of CDOM

This quantity varies with the ratio of suspended matter to the CDOM: according to (1), at constant b_b, λ_{max} shifts to the red with the content of CDOM in water because absorption coefficient of the latter exponentially grows with diminishing wavelength. Suspended matter in waters of our testing site is dominated by relatively large particles because of their biological origination (Ferreira et al., 2013; Stramski et al., 2004). In this case, b_b is virtually independent of λ and CDOM abundance becomes the only cause of λ_{max} variability in the visible.

The concept of Case 1/Case 2 waters disregards two facts: (1) living algal cells release dissolved organic carbon (DOC) in

measurable quantities during log-phase growth (Chen and Wangersky, 1996a) and (2) this DOC might be highly labile to bacterial utilization and could be degraded significantly within hours (Chen and Wangersky, 1996b). The CDOM is a fraction of dissolved degradation products that absorbs light and emits fluorescence. The time scales of evolution of refractory CDOM considerably exceed the residence time of algal blooms induced by mesoscale dynamical events (from days up to 2–3 weeks). Thus, a bloom of algae is always accompanied by evolution of optically significant CDOM of algal origination.

This matters for remote determination of chlorophyll by means of band-ratio and band-difference algorithms. However, the first one relies on reflectances spaced in a wavelength scale by a hundred of nanometers while the band-difference algorithm for ALH determination involves violet-blue reflectances on each side of chlorophyll absorption peak at 443 nm. Hence, the ALH algorithm is tuned to the algae specific property while the band-ratio algorithms use much wider part of reflectance spectrum influenced by a number of natural admixtures in seawater, the products of algae degradation inclusive. These circumstances explain the similarity of patches of longer λ_{max} and higher *chl_a* in Figs. 4–8 and the dependence of *chl_a* distributions upon the λ_{max} in Fig. 10. Thus, the similarity of λ_{max} and *chl_a* in spatial distribution goes beyond the cases of mesoscale patches but is characteristic of the entire area of frequent occurrence of these inhomogeneities.

The products of degradation of a substance lag behind the evolution of substance itself by definition. It is reasonable to admit that co-existence of elevated λ_{max} with low C_{ALH} are indicative of senescent or extinct mesoscale algal blooms.

4.4. Origination of shortwave reflectance deficit

The absorption and backscattering spectra of non-pigment natural seawater admixtures in the visible appear as monotonous wavelength functions. Superposition of the latter results at best in a unimodal distribution of reflectance whose maximum shifts to the red with the content of CDOM in water (Jerlov, 1976). Undeniably, the chlorophyll and accessory phytoplankton pigments are the only seawater admixtures responsible for the shortwave reflectance minima because, firstly, they fall into the spectral range of absorption peaks of these pigments (Wozniak and Dera, 2007) and, secondly, their absorption considerably exceeds absorption of non-pigment natural admixtures in spectral selectivity.

It has been shown in the above Introduction that every instance of shortwave reflectance deficit in MODIS spectra took place at sites where algal cells accumulated near the water surface owing to various forcings. First, this is cell buoyancy tuning for surfacing in the case of cyanobacterial blooms. Second, the internal tide served as a driver of bloom in the Kerguelen area (Park et al., 2008) where the Circumpolar Current branch attacks the slope of the underwater plateau and, hypothetically, gives rise to an orographic upwelling that enhances the tide effect. Third, a quasi-permanent upwelling over the shelfbreak triggers the phytoplankton bloom hundreds of miles long and visible as a frequent feature in satellite images off the Patagonian shelf (Garcia et al., 2008; Matano and Palma, 2008).

Fig. 8 shows the TS part where NSMs occurred against a background of water exchange between the local waters and the Malvinas Current (low SST in map (a)). The latter comes from higher latitudes, where waters are colder and richer in CDOM (Nelson et al., 2010) relative to the BMCZ waters of moderate latitudes. Thus, the lower SST marks the outcroppings of Malvinas Current waters or their mixture with local waters because the SST signal originates in the skin layer of a water body. The shapes in Fig. 8 demonstrate various mesoscale patterns resulting from interaction of intruding and local waters. Loop L in map (a) coincides in space with well discriminable loops in the fields of λ_{max} (map (b)) and *chl_a* (map (c)). The same loop L is traced by medium level estimates of R_{rs} (555) (map(e)) but vanishes in the field of C_{ALH} (map (f)). In contrast, the shape of eddy-like structure E is reproduced by higher estimates of R_{rs}(555) (map (e)) and C_{ALH} (map (f)). To all appearance, this is a consequence of algal bloom induced by eddy E in the zone of horizontal water exchange between the northwards flowing Malvinas Current and warmer offshore waters. These patterns point to meso- and sub-mesoscale scale water dynamics near the air-water interface as the fourth ubiquitous cause of non-zero ALH estimates in Case 1 waters. Our interpretation is consistent with recent findings concerning the impact of mesoscale water dynamics on the primary production of the open ocean (Mahadevan, 2016; McGillicuddy et al., 2007).

4.5. C_{ALH} versus *chl_a* and FLH

Chlorophyll content in water retrieved from the sea surface reflectance is open to inacceptable bias if concentration of chlorophyll peaks below the layer of reflectance origination. The tentative thickness of this layer $Z = 1/K_d$ where K_d is the diffuse attenuation coefficient of solar radiation (Gordon and McCluney, 1975). According to Jerlov (1976), $Z \approx 55$ M in the clearest ocean water at $\lambda = 475$ nm. However, it has long been known that the chlorophyll maxima happen to be as deep as 100 m and deeper (Karabashev, 1987; McGillicuddy, 2001). In this respect, the ALH index offers no advantage over the multitude of algorithms appeared since late 1970s and based on the band-ratio approach (Blondeau-Patissier et al., 2014). However, the latter relies on empirical relation of reflectances that depend on a number of water constituents of elusive nature. In contrast, the ALH is obtainable from measured intensity of a physical phenomenon inherent to the substance to be determined. This approach corresponds to the principles of optical chemical analysis widely used in science and industry. The basic disadvantage of ALH-approach is higher scatter of chlorophyll determinations because the ALH is calculable as a difference of reflectances close in amplitude. To summaries, band-ratio methods are advantageous in lower output scatter while the ALH approach promises lower bias.

The ALH index is akin to the FLH index in that they are attributable to the chlorophyll as a water admixture. However, the former depends upon the absorption of light by chlorophyll while the latter is dependent on the same absorption plus the energy dissipation processes, the act of emitting fluorescence inclusive (Aiken, 2001). In the case of aquatic applications, at least three circumstances downgrade the

diagnostic potential of chlorophyll fluorescence as compared to the chlorophyll absorption of solar radiation.

(1) The chlorophyll fluorescence spectrum peaks at $\lambda \approx 678$ nm where water proper is the main contributor in seawater light absorption: in ocean waters at $\lambda = 675$ nm we have $0.42 < K_d < 0.52$ m^{-1} (Jerlov, 1976). Thus, $Z < 2.5$ m represents the thickness of origination layer of red reflectance round the ocean. In contrast, absorption bands of chlorophyll and accessory pigments of algae belong to the blue-green spectral range where remotely sensed reflectance originates from layers tens of meters thick in waters of high and moderate transparency (see above). As a result, the chlorophyll fluorescence from algal cells excited by shortwave solar radiation below 2.5 m depth level cannot be detected by ship-borne and satellite sensors throughout the World Ocean.
(2) The spectral resolution of multispectral sensors is too low to reliably avoid absorption features in the atmosphere and to resolve absorption and fluorescence bands of chlorophyll in the red (Letelier and Abbott, 1996).
(3) "The in vivo fluorescence (IVF) yield of chlorophyll has been reported to vary with species composition, size category, and time of day (IVF yields may be greater by a factor of 5 at night). Near-surface phytoplankton, in high light and with high photosynthetic activity, have reduced (quenched) IVF yield" (Aiken, 2001). This inconvenience is difficult to eliminate without resorting to ground truthing.

5. Conclusions

Analytical treatment of MODIS images of testing site in the Brazil-Malvinas Confluence Zone allowed us to:

(1) establish occurrence of reflectance NSM (reflectance deficit due to chlorophyll absorption) in the Brazil-Malvinas Confluence during austral summer,
(2) demonstrate association of reflectance NSM with the mesoscale dynamical structures and suitability of the NSM for indication of chlorophyll abundance in water,
(3) propose a new satellite indicator of chlorophyll abundance ALH (Absorption Line Height) based on reflectance minimum at 443 nm and calculable as linear interpolant of $R_{rs}(412)$ and $R_{rs}(469)$ to $\lambda = 443$ nm minus $R_{rs}(443)$,
(4) find the qualitative conformity of chlorophyll determinations in the BMCZ based on water sampling (Balch et al., 2014) with those based on linear dependence of the ALH upon chlorophyll concentration derived from the Caspian Sea ground truth data,
(5) reveal the informativeness of the multispectral λ_{max} as a measurable objective index of the CDOM impact on the reflectance spectrum of optically complex waters,
(6) propose a two-stage procedure for physical clustering the reflectance spectra of pixels of MODIS images based on evaluation of λ_{max} and the NSM characteristics.
(7) to demonstrate that the mesoscale structures in Case 1 waters are often accompanied by CDOM manifestations, which have no effect on ALH as index of chlorophyll abundance but are damaging for band-ratio algorithms for chlorophyll retrieving from multispectral reflectance of water surface.

Most likely, the index ALH will find use as a remote index of chlorophyll abundance in aquatic areas where phytoplankton accumulates just below the air-water interface due to adaptive behavior of algae, permanent water upwellings, and mesoscale water dynamics. The meso- and sub-mesoscale eddies are accepted as significant suppliers of nutrients into the photic layer of the ocean (McGillicuddy et al., 1998). It is felt that the ALH-based algorithm is advantageous in studies of eddy-driven blooms in Case 1 waters because it more adequately differentiates between the chlorophyll and by-products of algal life cycle. Hence, validation of trial solution (3) under the most diverse natural conditions is of crucial importance for implementing the results of the present paper.

The intermittency of spectral clusters within the testing site, the attribution of complex spectral shapes, and other previously mentioned phenomena deserve special consideration in parallel with efforts to squeeze out the maximum informativeness of the ALH index. This is particularly challenging in the case of blooms caused by the meso- and sub-mesoscale dynamical events because they are short-lived, sliding, and unpredictable. Our results can be useful for a qualitative analysis of the oceanological situation when preparing and supporting scientific biological-ecological expeditions and for exploration of oceanic fishing areas distinguished by considerable mesoscale variability.

Acknowledgments

The estimates of R_{rs}, chl_a, C_{ALH} and λ_{max} were retrieved from the L2 product of the MODIS Aqua available at the ocean color website (http://oceancolor.gsfc.nasa.gov/), NASA Goddard Space Flight Center, Ocean Ecology Laboratory, Ocean Biology Processing Group (Moderate-resolution Imaging Spectroradiometer (MODIS) Aqua Ocean Color Data; 2014).

This research was performed in the framework of the state assignment of FASO Russia (theme no. 0149-2018-0002).

References

Acha, E.A., Mianzan, H.W., Guerrero, R.A., Favero, M., Bava, J., 2004. Marine fronts at the continental shelves of austral South America. J. Mar. Syst. 44 (1–2), 83–105, http://dx.doi.org/10.1016/j.jmarsys.2003.09.005.

Aiken, J., 2001. Fluorometry for biological sensing. In: Steele, J.H., Turekian, K.K., Thorpe, S.A. (Eds.), Encyclopedia of Ocean Sciences. Acad. Press, London, 1695–1945, http://dx.doi.org/10.1006/rwos.2001.0338.

Balch, W.M., Drapeau, D.T., Bowler, B.C., Lyczkowski, E.R., Lubelczyk, L.C., Painter, S.C., Poulton, A.J., 2014. Surface biological, chemical, and optical properties of the Patagonian Shelf coccolithophore bloom, the brightest waters of the Great Calcite Belt. Limnol. Oceanogr. 59 (5), 1715–1732, http://dx.doi.org/10.4319/lo.2014.59.5.1715.

Barton, E.D., 2001. Island wakes. In: Steele, J.H., Turekian, K.K., Thorpe, S.A. (Eds.), Encyclopedia of Ocean Sciences. Acad. Press, London, 1397–1403, http://dx.doi.org/10.1006/rwos.2001.0338.

Blondeau-Patissier, D., Gower, J.F.R., Dekker, A.G., Phinn, S.R., Brando, V.E., 2014. A review of ocean color remote sensing methods and statistical techniques for the detection, mapping and analysis of phytoplankton blooms in coastal and open oceans. Progr. Oceanogr. 123, 123–144.

Chen, W., Wangersky, P.J., 1996a. Production of dissolved organic carbon in phytoplankton cultures as measured by high-temperature catalytic oxidation and ultraviolet photo-oxidation methods. J. Plankton Res. 18, 1201–1211, http://dx.doi.org/10.1093/plankt/18.7.1201.

Chen, W., Wangersky, P.J., 1996b. Rates of microbial degradation of dissolved organic carbon from phytoplankton cultures. J. Plankton Res. 18, 1521–1533, http://dx.doi.org/10.1093/plankt/18.9.1521.

Clarke, G.L., Ewing, G.C., Lorenzen, C.J., 1970. Spectra of backscattered light from the sea obtained from aircraft as a measure of chlorophyll concentration. Science 167 (3921), 1119–1121, http://dx.doi.org/10.1126/science.167.3921.1119.

d'Ortenzio, F., Marullo, S., Ragni, M., d'Alcalà, M.R., Santoleri, R., 2002. Validation of empirical SeaWiFS algorithms for chlorophyll-*a* retrieval in the Mediterranean Sea: A case study for oligotrophic seas. Remote Sens. Environ. 82 (1), 79–94, http://dx.doi.org/10.1016/S0034-4257(02)00026-3.

d'Ovidio, F., De Monte, S., Alvain, S., Dandonneau, Y., Levy, M., 2010. Fluid dynamical niches of phytoplankton types. PNAS 107 (43), 18366–18370.

Dupouy, C., Benielli-Gary, D., Neveux, J., Dandonneautelesc, Y., Westberry, T.K., 2011. An algorithm for detecting Trichodesmium surface blooms in the South Western Tropical Pacific. Biogeosciences 8, 3631–3647.

Ferreira, A., Stramski, D., Garcia, C.A.E., Garcia, V.M.T., Ciotti, A. M., Mendes, C.R.B., 2013. Variability in light absorption and scattering of phytoplankton in Patagonian waters: role of community size structure and pigment composition. J. Geophys. Res. Oceans 118 (2), 698–714, http://dx.doi.org/10.1002/jgrC.20082.

Garcia, C.A.E., Garcia, V.M.T., McClain, C.R., 2005. Evaluation of SeaWiFS chlorophyll algorithms in the Southwestern Atlantic and Southern Oceans. Remote Sens. Environ. 95, 125–137, http://dx.doi.org/10.1016/j.rse.2004.12.006.

Garcia, V.M.T., Garcia, C.A.E., Mata, M.M., Pollery, R.C., Piola, A.R., Signorini, S.R., McClain, C.R., Iglesias-Rodriguez, M.D., 2008. Environmental factors controlling the phytoplankton blooms at the Patagonia shelf-break in spring. Deep-Sea Res. Pt. I 55, 1150–1166, http://dx.doi.org/10.10l6/j.dsr.2008.04.011.

Georges, C., Monchy, S., Genitsaris, S., Christaki, U., 2014. Protist community composition during early phytoplankton blooms in the naturally iron-fertilized Kerguelen area (Southern Ocean). Biogeosciences 11, 5847–5863, http://dx.doi.org/10.5194/bg-11-5847-2014.

Gordon, H.R., McCluney, W.R., 1975. Estimation of the depth of sunlight penetration in the sea for remote sensing. Appl. Optics 14, 413–416.

Hu, C., Lee, Z., Franz, B., 2012. Chlorophyll *a* algorithms for oligotrophic oceans: a novel approach based on three-band reflectance difference. J. Geophys. Res. 117, C01011, http://dx.doi.org/10.1029/2011JC007395.

Jerlov, N.G., 1976. Marine Optics. Elsevier, Amsterdam, 233 pp.

Kalle, K., 1963. Über das Verhalten und die Herkunft der in den Gewässern und in der Atmosphäre vorhandenen himmelblauen Fluoreszenz. Deutsche Hydrografische Zeitschrift 16, 153–166.

Karabashev, G.S., 1987. Fluorescence in the Ocean. Gidrometeoizdat, Leningrad, http://dx.doi.org/10.13140/2.1.3439.7128, 200 pp., (in Russian).

Karabashev, G.S., Evdoshenko, M.A., 2015a. Spectral features of cyanobacterial bloom in the Baltic Sea from MODIS data. Sovremennye Problemy Distantsionnogo Zondirovaniya Zemli iz Kosmosa 12 (3), 158–170, (in Russian).

Karabashev, G.S., Evdoshenko, M.A., 2015b. On spectral indications of cyanobacteria blooms at ecologically different aquatic areas from satellite data. In: Proc. VIII Int. Conf. "Current Problems in Optics of Natural Waters" (ONW'2015), Saint-Petersburg, 171–176, http://dx.doi.org/10.13140/RG.2.1.2812.6161.

Karabashev, G.S., Evdoshenko, M.A., 2016. Narrowband shortwave minima in spectra of backscattered light from the sea obtained from ocean color scanners as a remote indication of algal blooms. Oceanologia 58 (5), 279–291, http://dx.doi.org/10.1016/j.oceano.2016.05.001.

Karabashev, G.S., Evdoshenko, M.A., 2017a. Shortwave minimums of reflectance of water surface as a remote indication of blooms of *Nodularia spumigena* in the southern Caspian Sea, 2017. Sovremennye Problemy Distantsionnogo Zondirovaniya Zemli iz Kosmosa 14 (1), 159–174, http://dx.doi.org/10.21046/2070-7401-2017-14-1-159-174 (in Russian).

Karabashev, G.S., Evdoshenko, M.A., 2017b. A new approach to satellite diagnostics of phytoplankton blooms from reflectance spectra of ocean surface. In: Proc. IX Int. Conf. "Current Problems in Optics of Natural Waters" (ONW'2017), Saint-Petersburg, 123–126.

Kopelevich, O.V., Burenkov, V.I., Goldin, Yu.A., Sheberstov, S.V., 2005. Bio-optical studies in the Atlantic ocean combining satellite and ship measured data. In: Proc. III Int. Conf. "Current Problems in Optics of Natural Waters" (ONW'20005), Saint-Petersburg, 193–198.

Kopelevich, O.V., Sheberstov, S.V., Sahling, I.V., Vazyulya, S.V., Burenkov, V.I., 2013. Bio-optical Characteristics of the Barents, White, Black, and Caspian Seas from Data of Satellite Ocean Color Scanners, http://optics.ocean.ru.

Letelier, R., Abbott, M., 1996. An analysis of chlorophyll fluorescence algorithms for the Moderate Resolution Imaging Spectrometer (MODIS). Remote Sens. Environ. 58, 215–223, http://dx.doi.org/10.1016/50034-4257(96)00073-9.

Loder, J.W., Boicourt, W.C., Simpson, J.H., 1998. Western ocean boundary shelves coastal segment (W). In: Robinson, A.R., Brink, K.H. (Eds.), The Sea, vol. 11. Wiley, New York, 3–27.

Lubac, B., Loisel, H., 2007. Variability and classification of remote sensing reflectance spectra in the Eastern English Channel and Southern North Sea. Remote Sens. Environ. 110, 45–58.

Mahadevan, A., 2016. The impact of submesoscale physics on primary productivity of plankton. Annu. Rev. Mar. Sci. 8, 161–184, http://dx.doi.org/10.1146/annurev-marine-010814-015912.

Matano, R.P., Palma, E.D., 2008. On the upwelling of downwelling currents. J. Phys. Oceanogr. 38, 2482–2500, http://dx.doi.org/10.1175/2008JPO3783.1.

Matano, R.P., Palma, A.R., Piola, A., 2010. The influence of the Brazil and Malvinas Currents on the Southwestern Atlantic Shelf circulation. Ocean Sci. 6, 983–995, http://dx.doi.org/10.5194/os-6-983-2010.

McClain, C., 2001. Ocean color from satellites. In: Steele, J.H., Turekian, K.K., Thorpe, S.A. (Eds.), Encyclopedia of Ocean Sciences. Acad. Press, London, 1695–1945, http://dx.doi.org/10.1006/rwos.2001.0338.

McGillicuddy Jr., D.J., 2001. Small-scale patchiness, models of. In: Steele, J.H., Turekian, K.K., Thorpe, S.A. (Eds.), Encyclopedia of Ocean Sciences. Acad. Press, London, 2820–2833, http://dx.doi.org/10.1006/rwos.2001.0405.

McGillicuddy Jr., D.J., Anderson, L.A., Bates, N.R., Bibb, T., Buesseler, K.O., Carlson, C.A., Davis, C.S., Ewart, C., Falkowski, P.G., Goldthwait, S.A., Hansell, D.A., Jenkins, W.J., Johnson, R., Kosnyrev, V.K., Ledwell, J.R., Qian, P. Li, Siegel, D.A., Steinberg, D.K., 2007. Eddy/wind interactions stimulate extraordinary mid-ocean plankton blooms. Science 316 (5827), 1021–1026, http://dx.doi.org/10.1126/science.1136256.

McGillicuddy Jr., D.J., Robinson, A.R., Siegel, D.A., Jannasch, H.W., Johnson, R., Dickey, T.D., McNeil, J., Michaels, A.F., Knap, A.H., 1998. Influence of mesoscale eddies on new production in the

Sargasso Sea. Nature 394 (6690), 263—266, http://dx.doi.org/10.1038/28367.

Mobley, C.D., Stramski, D., Bisset, W.P., Boss, E., 2004. Optical modeling of ocean water. Is the Case 1—Case 2 classification still useful? Oceanography 17 (2), 60—67.

Morel, A., 1988. Optical modeling of the upper ocean in relation to its biogenous matter content. J. Geophys. Res. 93 (10), 749—768, http://dx.doi.org/10.1029/JC093iC09p10749.

Morel, A., 2009. Are the empirical relationships describing the bio-optical properties of case 1 waters consistent and internally compatible? J. Geophys. Res. 114, C01016, http://dx.doi.org/10.1029/2008JC004803.

Morel, A., Huot, Y., Gentili, B., Werdell, P.J., Hooker, S.B., Franz, B. A., 2007. Examining the consistency of products derived from various ocean sensors in open ocean (Case 1) waters in the perspective of a multi-sensor approach. Remote Sens. Environ. 111, 69—88, http://dx.doi.org/10.1016/j.rse.2007.03.012.

Moreno, D.V., Pérez Marrero, J., Morales, J., Llerandi García, C., Villagarcía Úbeda, M.G., Rueda, M.J., Llinás, V., 2012. Phytoplankton functional community structure in Argentinian continental shelf determined by HPLC pigment signatures. Estuar. Coast. Shelf Sci. 100, 72—81.

Nelson, N.B., Siegel, D.A., Carlson, C.A., Swan, C.M., 2010. Tracing global biogeochemical cycles and meridional overturning circulation using chromophoric dissolved organic matter. Geophys. Res. Lett. 37, L03610, http://dx.doi.org/10.1029/2009GL042325.

Park, Y.-H., Fuda, J.-L., Durand, I., Garabato, S.C.N., 2008. Internal tides and vertical mixing over the Kerguelen Plateau. Deep-Sea Res. Pt. II 55, 582—593.

Piola, A.R., Matano, R., 2001. Brazil and Falklad (Malvinas) currents. In: Steele, J.H., Turekian, K.K., Thorpe, S.A. (Eds.), Encyclopedia of Ocean Sciences. Acad. Press, London, 340—349, http://dx.doi.org/10.1006/rwos.2001.0358.

Pope, R.M., Fry, E.S., 1997. Absorption spectrum (380—700 nm) of pure water. II. Integrating cavity measurements. Appl. Optics 36 (33), 8710—8723.

Sheberstov, S.V., 2015. System for batch processing of oceanographic satellite data. Sovremennye Problemy Distantsionnogo Zondirovaniya Zemli iz Kosmosa 12 (6), 154—161, (in Russian).

Stal, L.J., Albertano, P., Bergman, B., von Broeckel, K., Gallon, J.R., Hayes, P.K., Sivonen, K., Walsby, A.E., 2003. BASIC: Baltic Sea cyanobacteria. An investigation of the structure and dynamics of water blooms of cyanobacteria in the Baltic Sea—responses to a changing environment. Cont. Shelf Res. 23 (17—19), 1695—1714.

Stramski, D., Boss, E., Bogucki, D., Voss, K.J., 2004. The role of seawater constituents in light backscattering in the ocean. Prog. Oceanogr. (61), 27—56, http://dx.doi.org/10.1016/j.pocean.2004.07.001.

Telesca, L., Pierini, J.O., Lovallo, M., Santamaría-del-Angel, E., 2018. Spatio-temporal variability in the Brazil-Malvinas Confluence Zone (BMCZ), based on spectroradiometric MODIS-AQUA chlorophyll-*a* observations. Oceanologia 60 (1), 76—85, http://dx.doi.org/10.1016/j.oceano.2017.08.002.

Wozniak, B., Dera, J., 2007. Light Absorption in Sea Water. Springer Science, Business Media, New York, 463 pp.

Wozniak, S.B., Stramski, D., 2004. Modeling the optical properties of mineral particles suspended in seawater and their influence on ocean reflectance and chlorophyll estimation from remote sensing algorithms. Appl. Optics 43 (17), 3489—3503.